scientific reports

Check for updates

OPEN

Effects of multiple cations and sintering temperature on microstructure and dielectric properties in $Na_{1/2}Ln_{1/2}Cu_3Ti_4O_{12}$ (Ln = Sm and Eu) ceramic materials

Long-Fei Yuan[1]✉, Ting Zhang[2] & Dan-Dan Han[3]

$Na_{1/2}Eu_{1/2}Cu_3Ti_4O_{12}$ and $Na_{1/2}Sm_{1/2}Cu_3Ti_4O_{12}$ dielectric ceramics were synthesized at different sintering temperatures (950, 975 and 1000 °C) by a solid-state reaction method. Phase structure, cation valence state, and dielectric properties of all sintered ceramics were systematically investigated. When the preparation temperature was changed, the Cu^+ ion concentration of (Na^+, Eu^{3+}) co-doped ceramics changed faster than that of (Na^+, Sm^{3+}) co-doped ceramics. Abnormally high dielectric constants of ~ 3.17×10^4 and ~ 1.06×10^4 (at 10 Hz and 303 K) were achieved in $Na_{1/2}Sm_{1/2}Cu_3Ti_4O_{12}$ and $Na_{1/2}Eu_{1/2}Cu_3Ti_4O_{12}$ ceramics prepared at 950 °C, respectively. However, $Na_{1/2}Sm_{1/2}Cu_3Ti_4O_{12}$ and $Na_{1/2}Eu_{1/2}Cu_3Ti_4O_{12}$ prepared in high sintering temperature (1000 °C) exhibited a good frequency stability of dielectric permittivity. It was demonstrated that an increasing number of charge carriers induced by the increase of sintering temperature could lead to a competitive coexistence of two polarization mechanisms (surface barrier layer capacitor and internal barrier layer capacitor), further changing the dielectric properties of $CaCu_3Ti_4O_{12}$-based ceramics.

With the rapid development of network and information technology, the fifth generation (5G) network, online classroom and other technologies that are inseparable from people's lives are increasingly demanding the performance of capacitors, the basic components of electronic products[1–3]. Therefore, the research on the dielectric properties of different dielectric materials has always been a hot issue[4–7]. As a traditional dielectric material, $CaCu_3Ti_4O_{12}$ (CCTO) has been closely watched since its giant dielectric properties were found[8–11]. Two major aspects ways are used to optimize the dielectric properties of CCTO-like ceramics: (1) use of different preparation methods, for instance, solid-state reaction method[12], sol–gel[13], and spark plasma sintering[14], (2) the substitution of ions in the lattice, like La_2O_3[15], $Y_{2/3}Cu_3Ti_4O_{12}$[16],$Mg_{0.05}Al_{0.05}$[17], $Na_{1/2}Y_{1/2}Cu_3Ti_4O_{12}$[18], $Na_{1/2}La_{1/2}Cu_3Ti_4O_{12}$[19], $Ca_{1-x}Sr_xCu_3Ti_4O_{12-x}F_x$[20] and $Na_{1/3}Yb_{1/3}Ca_{1/3}Cu_3Ti_4O_{12}$[21], etc. Simultaneously, internal barrier layer capacitors (IBLC), as a major polarization mechanism, is used to explain the origin of dielectric behaviors for CCTO-based family materials[22,23].

The IBLC model is considered to be an internal capacitor composed of semiconductor grains surrounded by insulating grain boundaries, which has also been discovered in other dielectric materials, such as the $BaTiO_3$ type ceramics[24] and rutile TiO_2-related ceramics[25,26]. Among them, the conductivity level of grain and grain boundary plays an important role in IBLC effect, which is affected by the number of charge carriers in the ceramic. For example, a high dielectric constant and a low loss tangent observed in $Na_{1/3}Ca_{1/3}Bi_{1/3}Cu_3Ti_4O_{12}$ has been attributed to the electrically heterogeneous and comprised of semiconducting grains and insulating grain boundaries, while the semiconducting grains is primarily due to electron hopping between $Cu^+ \leftrightarrow Cu^{2+}$ and $Ti^{3+} \leftrightarrow Ti^{4+}$ sites[27]. The colossal dielectric of $Na_{1/2}Y_{1/2}Cu_3Ti_4O_{12}$ ceramic are closely related to the electrically heterogeneous microstructure at the insulating grain boundary, and the origin of semiconducting grains is likely correlated with the Cu_2O phase and the large amount of Ti^{3+}/Ti^{4+} ions[28]. For (Al^{3+},Nb^{5+}) co-doped $CaCu_3Ti_4O_{12}$ ceramics, the high dielectric permittivities with good temperature stability has been attributed to the internal

[1]College of Physics and Electronic Science, Zunyi Normal University, Zunyi 563002, Guizhou, China. [2]College of Chemistry and Chemical Engineering, Zunyi Normal University, Zunyi 563002, Guizhou, China. [3]College of Chemistry and Pharmaceutical Engineering, Jilin Institute of Chemical Technology, Jilin 132022, Jilin, China. ✉email: yuanlf2019@163.com

barrier layer capacitor model of Schottky barriers at grain boundaries, meanwhile electron hopping can occur in both Ti^{3+}–O–Ti^{4+} and Cu^{+}–O–Cu^{2+} ions[29].

It is obvious that the dielectric properties of CCTO-related ceramics can be effectively improved by the doping of ions, especially multiple cations (shown in the Table 1). But few reports explained the relationship between the preparation conditions (especially sintering temperature), grain conductivity, internal polarization mechanism, and dielectric properties of ceramics. Thus, it is fundamentally important to build a clear picture for the evolution of internal polarization mechanism along with the number of charge carriers in grain. Up to the present time, little work has been done on the sintering temperature, structural and dielectric properties of the signal phase (Na^{+}, Eu^{3+}) or (Na^{+}, Sm^{3+}) co-doped CCTO ceramics, specifically $Na_{1/2}Eu_{1/2}Cu_3Ti_4O_{12}$ and $Na_{1/2}Sm_{1/2}Cu_3Ti_4O_{12}$. Boonlakhorn et al. and Somphan et al. reported the good dielectric properties of $Na_{1/2}Sm_{1/2}Cu_3Ti_4O_{12}$ ceramics respectively, but a little impurity phase of $Sm_4Ti_3O_{12}$ or CuO was detected in ceramics[31,32]. Considering the comparison with Sm doped $ACu_3Ti_4O_{12}$ ceramics, the Eu ion closest to Sm in the periodic table of the elements was selected as doping ion to study the polarization mechanism and dielectric properties for CCTO-related ceramics. And, there is no discussion on the relationship between sintering temperature, the number of charge carriers, polarization mechanism and dielectric properties of $Na_{1/2}Eu_{1/2}Cu_3Ti_4O_{12}$ and $Na_{1/2}Sm_{1/2}Cu_3Ti_4O_{12}$ ceramics. A better understanding of the effect of polarization mechanism could be helpful for designing oxide ceramics with superior dielectric properties.

In this study, the $Na_{1/2}Ln_{1/2}Cu_3Ti_4O_{12}$ (Ln = Eu or Sm) ceramics were synthesized by solid-state reaction. The relationship among microstructure, polarization mechanism and dielectric properties of $Na_{1/2}Ln_{1/2}Cu_3Ti_4O_{12}$ (Ln = Eu or Sm) ceramics had been conformed for the first time by carefully tuning the number of charge carriers in grain via the change of sintering temperature. It could be notable that the sintering temperature altered the number of charge carriers in grain, induce different polarization mechanism, resulting in varied dielectric properties of the $Na_{1/2}Ln_{1/2}Cu_3Ti_4O_{12}$ ceramics.

Materials and methods

Sample preparation. $Na_{1/2}Eu_{1/2}Cu_3Ti_4O_{12}$ and $Na_{1/2}Sm_{1/2}Cu_3Ti_4O_{12}$ ceramics were prepared via a solid state reaction method. The raw materials, TiO_2 (99.99%), CuO (99.95%), $CaCO_3$ (99.9%), Eu_2O_3 (99.9%) and Sm_2O_3 (99.9%) were carefully weighed and milled. First, the green pellets obtained with a uniaxial press were calcined at 600 °C for 10 h in air. The calcined pellets were ground into powders, and the obtained powders were pressed into pellets again. Then, the ceramic samples were obtained by sintering compacted powder at different temperatures from 950 to 1000 °C for 10 h. For clarity, the obtained ceramics are named based on the composition ($Na_{1/2}X_{1/2}Cu_3Ti_4O_{12}$ expressed as N*X*CTO), and the sintering temperature (T in °C) as N*X*CTO-T. For example, the $Na_{1/2}Eu_{1/2}Cu_3Ti_4O_{12}$ ceramic sintered at 950 °C is named as NECTO-950.

Characterization. Crystal structure of these samples characterized using Powder X-ray diffraction (XRD) with a D8-focu Bruker apparatus (Cu Kα, λ = 0.15418 nm). The structural study was further performed by Raman spectra (RS) using a T64000 instrument under a 532 nm laser beam. The microstructural texture, and oxidation states were also analyzed by canning electron microscope (SEM) (FEI XL-30, America) and X-ray photoelectron spectroscopy (XPS, Escalab 250XI), respectively. The C1*s* photoemission line (284.6 eV) was used to calibrate the positions of the photoelectron spectra.

All pellets were carefully polished, and then coated surfaces with an Au layer film using a LJ-16 sputter coating unit. The dielectric properties of the ceramics were measured using a dielectric spectrometer (Novocontrol Concept 41) over the frequency and temperature ranges of 10 to 2×10^7 Hz and − 70 to 200 °C.

Samples	Preparation method	Sintering conditions	Mean grain size (μm)	Dielectric constant (1 kHz)	Dielectric loss (1 kHz)	References
$Bi_{1/2}Na_{1/2}Cu_3Ti_4O_{12}$	Pechini method	1000 °C for 10 h	3.2	2.77×10^3	0.11	[30]
$Na_{1/2}Bi_{1/2}Cu_3Ti_4O_{12}$	Sol–gel	1000 °C for 3 h	2.2	$\approx 10^4$	–	[9]
$Na_{1/3}Ca_{1/3}Bi_{1/3}Cu_3Ti_4O_{12}$	Solid state method	1060 °C for 5 h	2–20	2.59×10^4	0.038	[27]
$Na_{1/2}Sm_{1/2}Cu_3Ti_4O_{12}$	Sol–gel	1050 °C for 18 h	3.67	8.04×10^3	0.045	[31]
$Na_{1/2}Sm_{1/2}Cu_3Ti_4O_{12}$	Solid state method	1110 °C for 10 h	–	7.02×10^3	0.041	[32]
$Na_{1/2}La_{1/2}Cu_3Ti_4O_{12}$	Solid state method	1080 °C for 5 h	2–4	6.1×10^3	0.037	[33]
$Na_{1/2}La_{1/2}Cu_3Ti_4O_{12}$	Spark plasma sintering	925 °C for 10 min	0.3	$> 10^3$	–	[14]
$Na_{1/2}Y_{1/2}Cu_3Ti_4O_{12}$	Solid state method	1085 °C for 5 h	11	1.4×10^4	0.04	[18]
$Na_{1/2}Y_{1/2}Cu_3Ti_4O_{12}$	Solid state method	1110 °C for 10 h	10.32	1.8×10^4	0.03	[28]
$Na_{1/2}Y_{1/2}Cu_3Ti_{4.1}O_{12}$	Solid state method	1090 °C for 5 h	4.06	2.56×10^4	0.022	[8]
$(Na_{1/3}Ca_{1/3}Yb_{1/3})Cu_3Ti_4O_{12}$	Sol–gel	1075 °C for 12 h	0.18–0.4	5488	0.075	[21]
$Na_{1/2}Sm_{1/2}Cu_3Ti_4O_{12}$	Solid state method	1000 °C for 10 h	19.73	5.5×10^3	0.055	This work
$Na_{1/2}Eu_{1/2}Cu_3Ti_4O_{12}$	Solid state method	1000 °C for 10 h	16.9	4.7×10^3	0.066	This work

Table 1. Sintering process, mean grain size and dielectric properties of some $LnCu_3Ti_4O_{12}$ (Ln = $Na_{1/2}Bi_{1/2}$, $Na_{1/2}Sm_{1/2}$, $Na_{1/2}Eu_{1/2}$, $Na_{1/2}La_{1/2}$, $Na_{1/2}Y_{1/2}$, $Na_{1/3}Ca_{1/3}Bi_{1/3}$ and $Na_{1/3}Ca_{1/3}Yb_{1/3}$ etc.) ceramics.

Results and discussion

X-ray diffraction analysis. Sintered $Na_{1/2}Eu_{1/2}Cu_3Ti_4O_{12}$ and $Na_{1/2}Sm_{1/2}Cu_3Ti_4O_{12}$ ceramics were first characterized using an XRD technique to confirm its phase structures. Figure 1a demonstrates the XRD patterns of the NECTO and NSCTO ceramics sintered under various temperatures from 950 to 1000 °C. A main phase of $CaCu_3Ti_4O_{12}$ (JCPDS 75-2188) with a cubic structure was defected in all ceramic samples. No impurity phase was observed. As shown in the Fig. 1b, the (220) peak shifts to a lower degree with increasing sintered temperature in the NECTO and NSCTO samples. The relevant lattice parameters, *a*, were calculated from the XRD patterns. The *a* values of the $CaCu_3Ti_4O_{12}$ was 7.391 Å[21]. The *a* values of the NECTO and NSCTO ceramics sintered at 950 °C were respectively found to be 7.379 and 7.381 Å, respectively. The lattice parameters (*a*) of NECCTO-950 and NSCCTO-975 were slightly smaller than that of $CaCu_3Ti_4O_{12}$, which was due to the small difference in the ionic radii in Na^+ ($r_{Na^+}=1.39$ Å), Sm^{3+} ($r_{Sm^{3+}}=1.24$ Å), Eu^{3+} ($r_{Eu^{3+}}=1.12$ Å) and Ca^{2+} ($r_{Ca^{2+}}=1.34$ Å).

Although the radius of Na^+ ion is larger than that of Ca^{2+}, the lattice of NECCTO-950 and NSCCTO-950 sample shrined with the occupation of Sm^{3+} and Eu^{3+} ions with a smaller radius in the CCTO-type structure. The *a* values of the NECTO and NSCTO samples sintered at 975 and 1000 °C were 7.388, 7.399 and 7.387, 7.392 Å, respectively. Interestingly, *a* values of the NECTO and NSCTO samples sintered at high temperature were significantly larger than that of ceramics prepared at low temperature, which could be attributed to the change in the cation valence state in the rutile crystal structure.

Raman spectrogram analysis. Raman spectra of NECTO and NSCTO pellets sintered at different temperature are depicted in Fig. 2a,b. In Fig. 2, five modes at around 153, 358, 450 and 552 cm^{-1} were observed for six ceramics, in agreement with previous reports[10]. The Raman active modes of NECTO and NSCTO ceramics, like $CaCu_3Ti_4O_{12}$, could be similarly expressed as $\Gamma_{Raman}=2A_g+2E_g+4F_g$[34]. These Raman modes corresponded to F_g (1), A_g (1), A_g (2) and F_g (3), respectively. Among these modes, the A_g (1), A_g (2) and F_g (1) modes was attributed to TiO_6 rotation like lattice vibrations, and the F_g (3) mode was associated with an O–Ti–O antistretching lattice vibrations.

Microstructure. The microstructures of the NECTO-950, NECTO-975, NECTO-1000, NSCTO-950, NSCTO-975 and NSCTO-1000 are shown in Fig. 3a–f, respectively. The mean grain size of all the ceramics are revealed in Fig. 4a. Figure 3 shows that all the ceramic samples had a relatively dense microstructure. Grains and grain boundaries were clearly observed. However, a very small amount of pores appeared on the microscopic surface for the ceramic samples sintered in the low temperature (e.g. NECTO-950, NECTO-975, NSCTO-950 and NSCTO-975). To study the microscopic surface for the NECTO and NSCTO ceramics sintered at different temperature, as shown in Fig. 4a, it was found that the sintering temperature had a significant influence on the microstructure. The results showed that the mean grain size of $Na_{1/2}Eu_{1/2}Cu_3Ti_4O_{12}$ samples prepared at various temperature increased slightly as the sintering temperature increased from 950 to 1000 °C, ≈ 5.93, ≈ 11.32, ≈ 16.9 μm, respectively. Similarly, the mean grain size of NSCTO ceramics also increased with the increase of sintering temperature. The change in the grain size of the ceramics is usually associated with the liquid phase

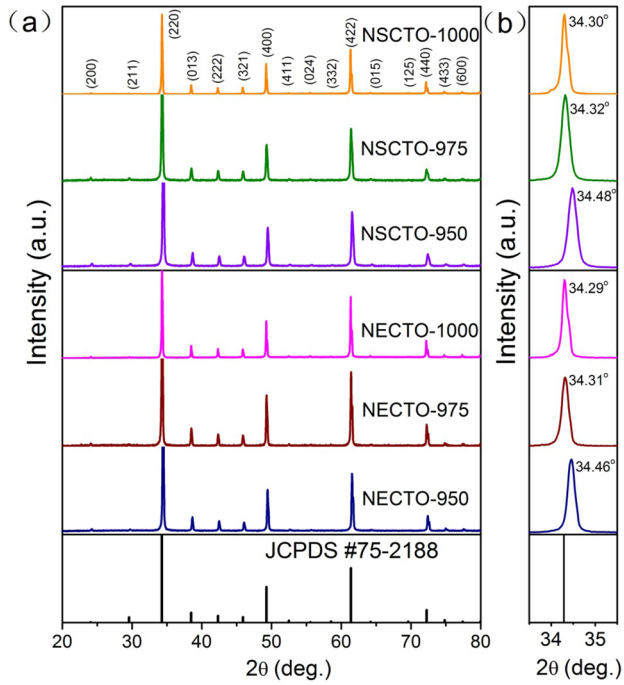

Figure 1. (**a**) XRD patterns of $Na_{1/2}Eu_{1/2}Cu_3Ti_4O_{12}$ and $Na_{1/2}Sm_{1/2}Cu_3Ti_4O_{12}$ ceramics sintered under different temperature; (**b**) changes of (220) diffraction peaks of these ceramic samples.

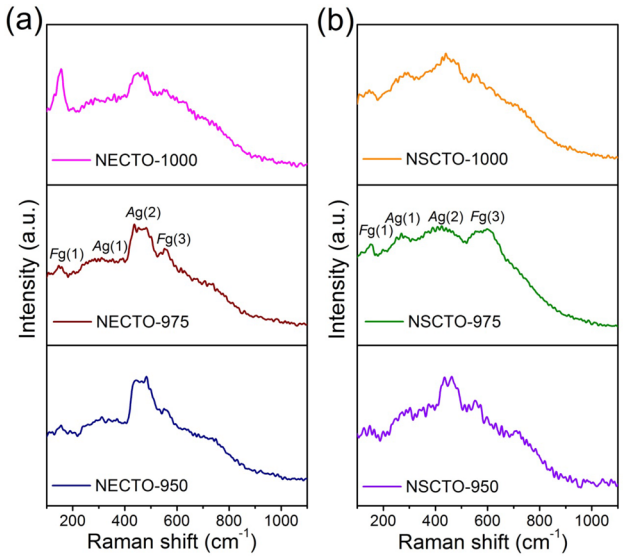

Figure 2. Raman spectra of (**a**) $Na_{1/2}Eu_{1/2}Cu_3Ti_4O_{12}$ and (**b**) $Na_{1/2}Sm_{1/2}Cu_3Ti_4O_{12}$ ceramics samples prepared in different sintering temperatures.

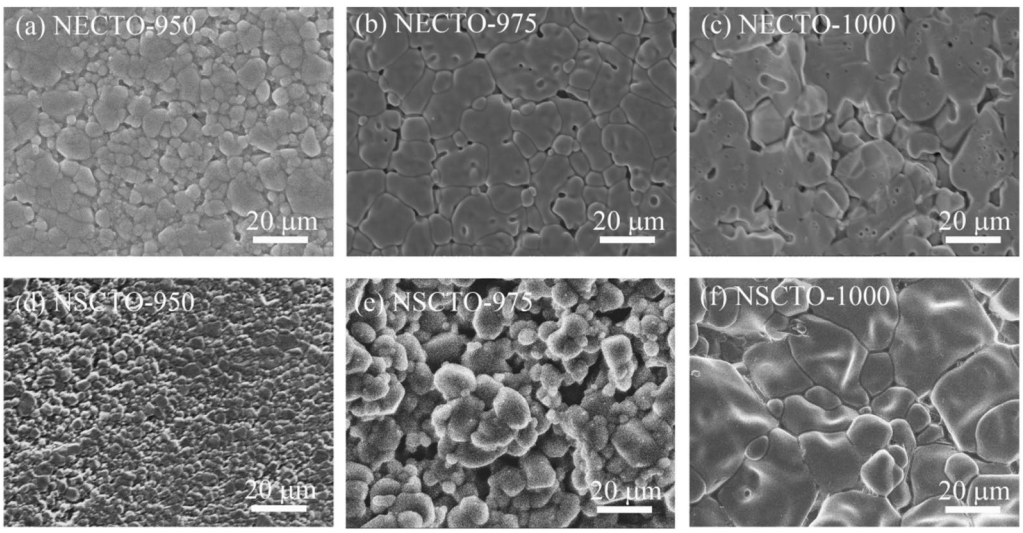

Figure 3. SEM images of $Na_{1/2}Eu_{1/2}Cu_3Ti_4O_{12}$ and $Na_{1/2}Sm_{1/2}Cu_3Ti_4O_{12}$ ceramics sintered under various temperature: (**a**) NECTO-950, (**b**) NECTO-975, (**c**) NECTO-1000, (**d**) NSCTO-950, (**e**) NSCTO-975 and (**f**) NSCTO-1000.

sintering mechanism, as reported in other CCTO-related ceramics[30,35–37]. However, in case of the NSCTO ceramics, the microstructure largely changed when the sintering temperature changed by only 25 °C. This phenomenon was similar to the $Na_{1/2}Ln_{1/2}Cu_3Ti_4O_{12}$-type ceramics reported by other researchers (shown in the Table 1). When the doping elements of $Na_{1/2}Ln_{1/2}Cu_3Ti_4O_{12}$-type ceramics changed from Y, La, Sm, Yb to Bi, the grain size of the prepared ceramics also showed significant changes. It may be related to the state of the extranuclear electron of the element. The Sm element is one atomic number lower than the Eu element, and the electrons of the 4f electron orbit are also one less, which may result in different grain growth trends of the NSCTO and NECTO ceramics under the same preparation conditions. The density of the samples has been measured by Archimedes method. As sintering temperature increased, the relative density of the NECTO ceramics increased monotonically from 83% for T = 950 °C and 87% for T = 975 °C to 91% for T = 1000 °C. And the relative density of NSCTO ceramics also increased with sintering temperature, reaching 81%, 85% and 92%, respectively.

XPS analysis. To identify the oxidation states of the polyvalent cations, the XPS spectrum was corrected. Figures 5 and 6 displayed the spectra of Ti 2*p*, Cu 2*p* for NECTO and NSCTO ceramics sintered at different temperature. Meanwhile, atomic ratios of Cu^{+}/Cu^{2+} and Ti^{3+}/Ti^{4+} estimated by XPS analysis were shown in the Fig. 4b in order to study the change of variable valence ion content in these ceramic samples. As presented in

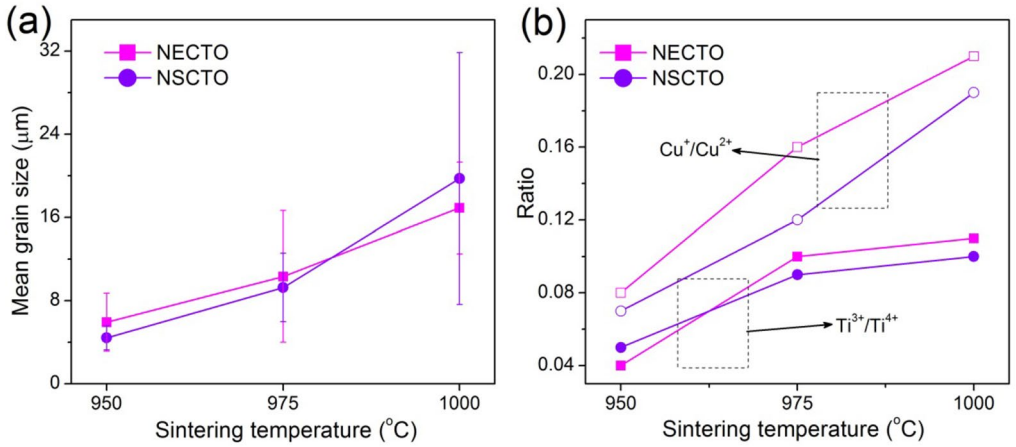

Figure 4. (**a**) Curves of mean grain size vs. sintering temperature for $Na_{1/2}Eu_{1/2}Cu_3Ti_4O_{12}$ and $Na_{1/2}Sm_{1/2}Cu_3Ti_4O_{12}$ ceramics. (**b**) Relationship between the atomic ratio of Cu^+/Cu^{2+} or Ti^{3+}/Ti^{4+} and sintering temperature for these samples. Solid dots and hollow dots in (**b**) correspond to the ratio of Ti^{3+}/Ti^{4+} and the ratio of Cu^+/Cu^{2+}, respectively.

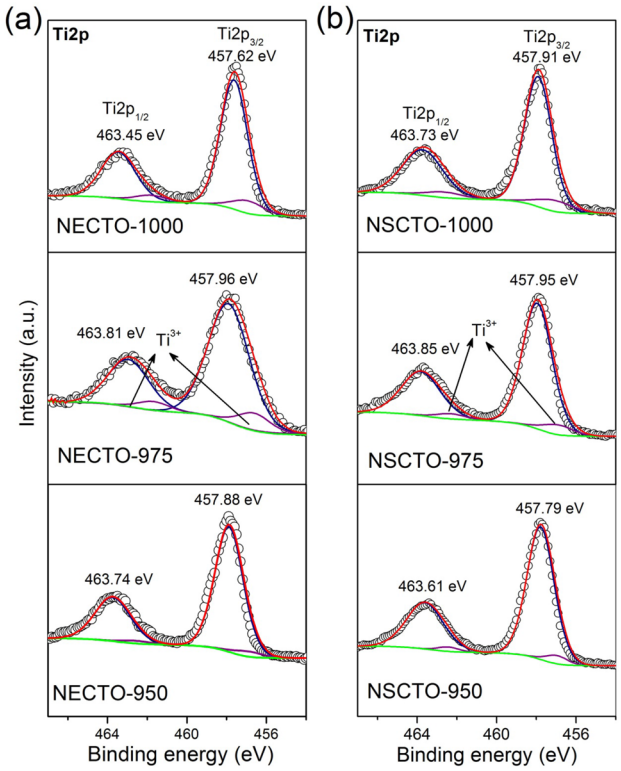

Figure 5. XPS spectra for the Ti 2*p* region for the (**a**) $Na_{1/2}Eu_{1/2}Cu_3Ti_4O_{12}$ and (**b**) $Na_{1/2}Sm_{1/2}Cu_3Ti_4O_{12}$ ceramics prepared at different sintering temperature.

Fig. 5, two asymmetrically shaped Ti $2p_{3/2}$ and Ti $2p_{1/2}$ are observed, indicating overlapping peaks of Ti^{3+} and Ti^{4+} ions[30,33,38]. According to the Gaussian–Lorentzian profile fitting, four peaks were obtained as displayed in the Fig. 5. This was observed in all sintered ceramics. For the intensive peak Ti $2p_{3/2}$ of NECTO and NSCTO ceramics, binding energy positions defining Ti^{3+} and Ti^{4+} were ~ 456.55–456.98 eV and ~ 457.62–457.96 eV, respectively. Figure 4b shows the radios of Cu^+/Cu^{2+} or Ti^{3+}/Ti^{4+} for NECTO and NSCTO ceramics. It was clearly that the content of Ti^{3+} ions in NECTO and NSCTO ceramics sintered in low temperature (950 °C) maintained a minor amount, and it increased slightly with the increase of sintering temperature.

Simultaneously, the Cu 2*p* spectrum in Fig. 6 indicate the presence of Cu^+. The main signal corresponding to Cu $2p_{3/2}$ of all ceramic samples could be deconvoluted into two signals: the binding energy positions of Cu^+ and

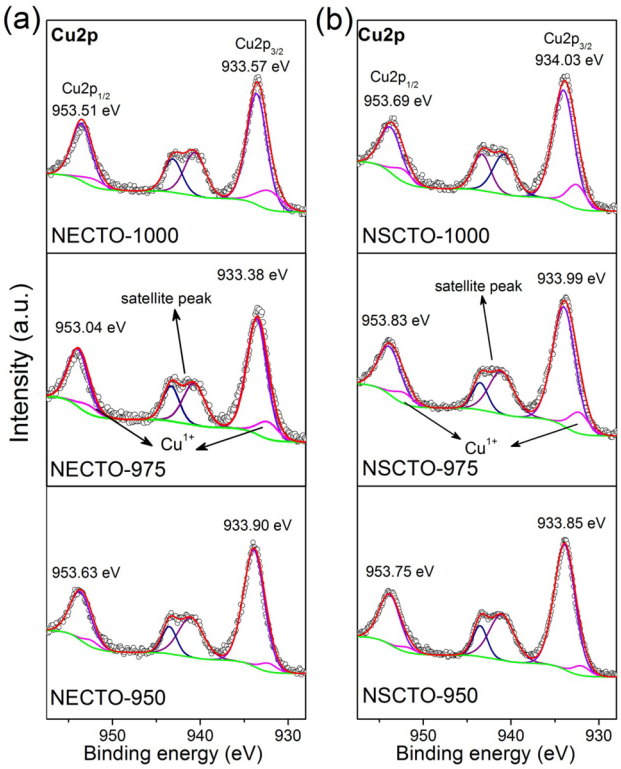

Figure 6. XPS spectra for the Cu 2*p* region for the (**a**) $Na_{1/2}Eu_{1/2}Cu_3Ti_4O_{12}$ and (**b**) $Na_{1/2}Sm_{1/2}Cu_3Ti_4O_{12}$ ceramics prepared at different sintering temperature.

Cu^{2+} are ~ 932.1–932.56 eV and ~ 933.38–934.03 eV, respectively. That is similar to that reported in the literature for CCTO and TiO_2-related ceramics[16,39,40]. The appearance of Ti^{3+} and Cu^{+} detected in $Na_{1/2}Eu_{1/2}Cu_3Ti_4O_{12}$ and $Na_{1/2}Sm_{1/2}Cu_3Ti_4O_{12}$ ceramics might have been related to the charge compensation caused by oxygen loss in its lattice structure during the sintering process[5,41]. As shown in the Fig. 4b, the concentration of Cu^{+} in NECTO and NSCTO ceramics samples significantly increased with the rise of sintering temperature, which was different from that of Ti^{3+} in these ceramics.

Simultaneously, it could be clearly confirmed that the content of Cu^{+} in (Na^{+}, Eu^{3+}) co-doped CCTO ceramics was generally higher than that in (Na^{+}, Sm^{3+}) co-doped CCTO ceramics for calcium copper titanate related ceramics, which may be related to the different electronic structures of Eu and Sm elements. Obviously, the ionic radius of the low valence state was larger than it of the high valence state. Therefore, the lattice structure of ceramics expands and the lattice parameters increase with the reduction of Cu^{2+} and Ti^{4+} in the grains. The NECTO-1000 and NSCTO-1000 samples with high concentration of Cu^{+} ions had the higher lattice parameters than other ceramics samples, which corresponded to the results observed by XRD.

Dielectric properties. In order to comprehend how the sintering temperature and mixing ions affects the dielectric responses, frequency dependences of dielectric constant (ε′) and dielectric loss (tan δ) for all samples at room temperature are shown in Fig. 7. Clearly, the overall frequency dependent behaviors of the NECTO and NSCTO ceramics differed obviously. As shown in Fig. 7a, ε′ of NSCCTO-950 sample rapidly decreased from 16,116 to 881 as frequency increased in the low frequency region. This is similar to that observed in NECTO-950 and NSCTO-975 ceramics also prepared at low sintering temperature. However, the permittivity was nearly independent of frequency from 10 to 10^6 Hz for NECTO-975, NECTO-1000 and NSCTO-1000 samples. Notably, the frequency stabilities of ε′ for NECTO-1000 and NSCTO-1000 samples were better than that of the NECTO-975 sample. The drastic decrease of dielectric constants for these samples at high frequency (> 10^6 Hz) could be attributed to the interfacial space charge polarization[16]. Figure 7b shows that the tan δ value of the NECTO-975, NECTO-1000 and NSCTO-1000 ceramics in the low frequency were obviously smaller than that of the NECTO-950, NSCTO-950 and NSCTO-975 ceramics. The peaks of dielectric loss (tan δ) for NECTO-950, NSCTO-950 and NSCTO-975 ceramics are presented at low frequencies. The tan δ values at 303 K and 1 kHz of the NECTO-950, NECTO-975, NECTO-1000, NSCTO-950, NSCTO-975 and NSCTO-1100 ceramics were approximately 0.285, 0.041, 0.066, 1.841, 1.407 and 0.055, respectively. Notably, When (Na^{+}, Eu^{3+}) or (Na^{+}, Sm^{3+}) was co-doped in CCTO-related ceramic prepared at high sintering temperature (975 or 1000 °C), the ceramic could retain low tan δ value and giant permittivity with good frequency stability.

The frequency of real part ε′ and imaginary part ε″ for NECTO and NSCTO ceramics at different temperature were shown in the Fig. 8 and its insets. Three plateau characteristics in the plots of ε′ versus frequency were

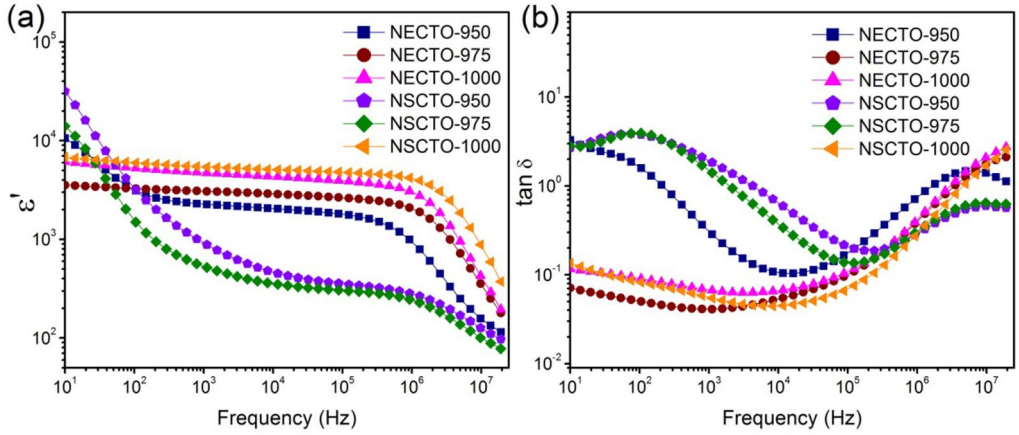

Figure 7. (**a**) Dielectric constant (ε′) and (**b**) dielectric loss (tan δ) at 303 K as a function of frequency for $Na_{1/2}Eu_{1/2}Cu_3Ti_4O_{12}$ and $Na_{1/2}Sm_{1/2}Cu_3Ti_4O_{12}$ ceramics sintered at different temperature.

observed in the temperature range from 203 to 443 K, which corresponded to three main parts of dielectric responses, respectively. The first plateau in a low frequency range was observed at the high temperature, which is attributed to an sample-electrode interface response[21,36]. In the low frequency region, as the test temperature increased, the dielectric constant changed more sharply with frequency, indicating that the sample-electrode interface response, i.e. the surface barrier layer capacitor (SBLC) polarization mechanism, was more obvious. Therefore, as shown in Fig. 8, there was a strong SBLC effect inside the NECTO-950, NECTO-975 and NSCTO-950 ceramics prepared at low sintering temperature, which leads to the abnormal high dielectric constant of these ceramics in the low-frequency region (shown in the Fig. 7a). As the Fig. 7b, the dielectric loss peaks of these three ceramics observed at low frequencies were also related to the SBLC effect. The primary plateau observed at intermediate frequency was attributed to the dielectric response of the grain boundaries[27,42], which was evident in the NECTO-1000, NSCTO-1000, and NECTO-975 ceramics prepared at high sintering temperature. However, the high frequency plateau observed at the low testing temperature was originated from the bulk response[23]. The dielectric responses of these three parts were clearly observed in CCTO-related ceramics[27,42,43]. As shown in the Fig. 8 insets, the peak of ε″ shifted to higher frequencies with increasing temperature, indicating that the dielectric relaxation process was thermally activated. It was found that the high frequency relaxation activation energies of the NECTO-950, NECTO-975, NECTO-1000, NSCTO-950, NSCTO-975, NSCTO-1000 ceramics were 0.116, 0.106, 0.102, 0.114, 0.113 and 0.100 eV, respectively. These activation energies were related to the electric response of the bulks or grains, which were similar to other CCTO-like ceramics[44–46].

Impedance spectroscopy analysis. To describe the dielectric behaviors of these ceramics, the impedance spectroscopy for NECTO and NSCTO ceramics was employed to illuminate this. In Fig. 9 and its inset, the linear part of the semicircular arcs with nonzero intercept on the Z′ axis was observed at 283 K. However, the semicircular arcs became apparent in low frequency region for NECTO-950, NSCTO-950 and NSCTO-975 ceramics (Fig. 9). For, CCTO-related ceramics, these electrical response are associated with the contributions from grain boundaries and grains, respectively[47].

The resistance values of grain, grain boundary and surface for NECTO and NSCTO ceramics were estimated using the equivalent R(RQ) circuit[23] shown in Table 2. As displayed in the Table 2, the grain resistance (R_g) values of these $Na_{1/2}Ln_{1/2}Cu_3Ti_4O_{12}$ (Ln = Eu or Sm) ceramics evidently decreased with increasing sintering temperature. The variation of R_g values for these ceramics was related to the appearance of low valent ions (Cu^+ and Ti^{3+}) at the grain during high-temperature sintering process[14,21,31].

Combined with XPS data, the Cu^+ and Ti^{3+} ions were prone to occur in ceramics due to the occupation of multiple cations (Na^+, Eu^{3+}) or (Na^+, Sm^{3+}) in CCTO-related ceramics. The higher the sintering temperature, the higher the concentration of low-valence ions (Cu^+ and Ti^{3+}) in NECTO or NSCTO ceramic (shown in the Fig. 4b), and the higher the conductivity of the grain. Hence R_g of NECTO-975, NECTO-1000 and NSCTO-1000 samples was much smaller than that of the other samples. The semiconducting conduction of grain in these samples was highly related with the electron hopping between $Cu^+ \leftrightarrow Cu^{2+}$ and $Ti^{3+} \leftrightarrow Ti^{4+}$. However, we have found that R_{gb} values of the $Na_{1/2}Ln_{1/2}Cu_3Ti_4O_{12}$ (Ln = Eu or Sm) ceramics increased significantly with the rise of sintering temperature. The insulation of grain boundaries may be related to the enrichment of Cu at grain boundaries in these ceramics, which has been observed in other ACTO-type ceramics[8,15,35,48]. Moreover, the high insulating grain boundaries could reduce the dielectric loss of the ceramic materials[14]. So the NECTO-975 ceramic with the highest grain boundary resistance in the NECTO system had the lowest dielectric loss about 0.041 at 303 K and 1 kHz (observed in Fig. 7b). Similarly, the NSCTO-1000 ceramic in the NSCTO series also had the lowest dielectric loss about 0.055 (at 303 K and 1 kHz). It was clearly demonstrated that R_g was more than 5 orders of magnitude smaller than R_g for NECTO-975, NECTO-1000 and NSCTO-1000 samples. Hence this suggests that the origin of giant dielectric response of these ceramics sintered in high temperature was correlated with a typical IBLC polarization mechanism.

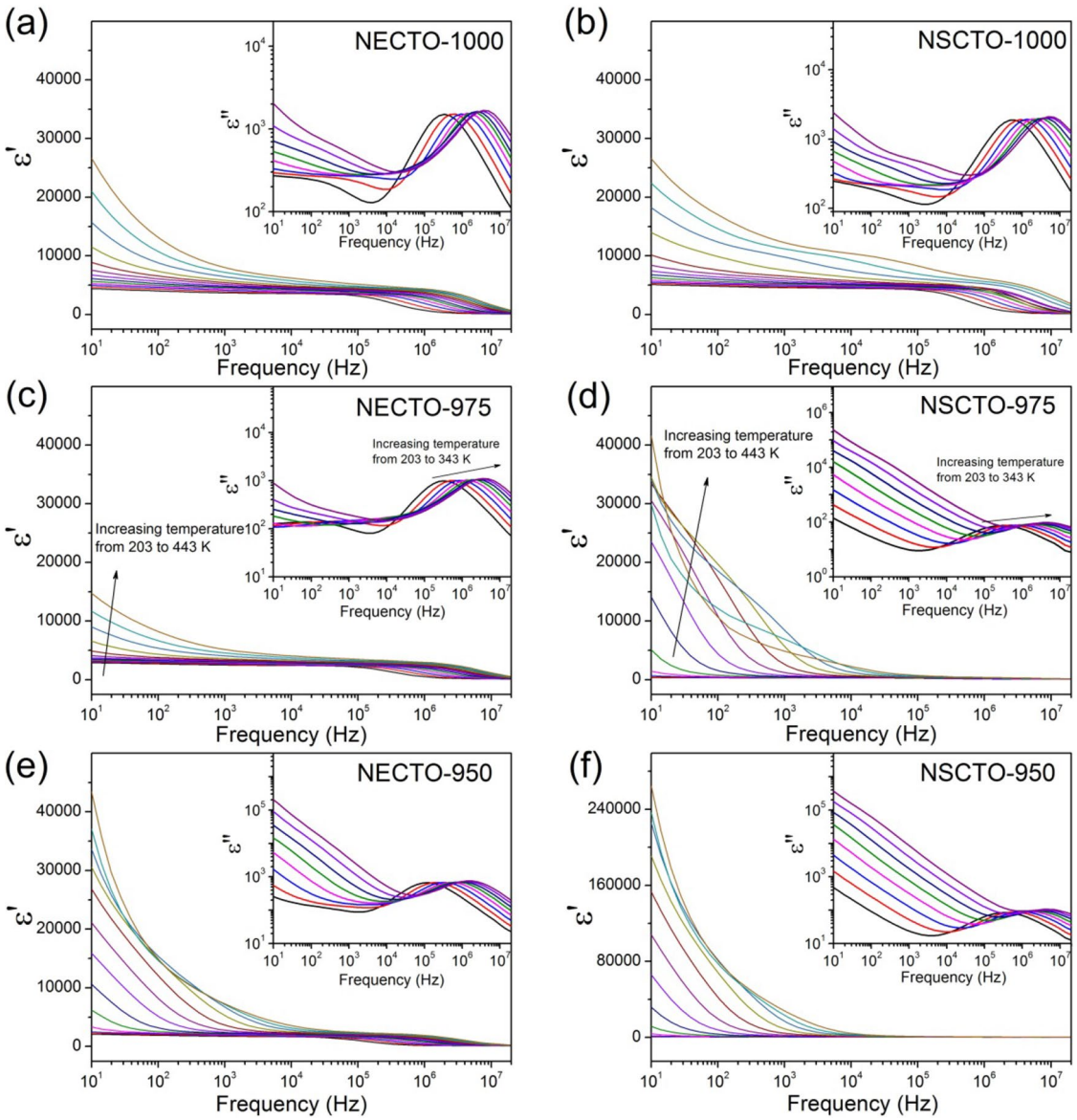

Figure 8. Frequency dependence of ε′ at various temperatures for (**a**) NECTO-1000, (**b**) NSCTO-1000, (**c**) NECTO-975, (**d**) NSCTO-975, (**e**) NECTO-950 and (**f**) NSCTO-950; their insets show the frequency dependence of ε″ in a temperature range from 203 to 343 K.

To optimize the results, the temperature dependence of AC conductivities (σ_{AC}) was measured in the temperature range of 103–473 K for NECTO and NSCTO ceramics, as illustrated in Fig. 10. Moreover, the activation energy required for the AC conductivities of charge carriers in the grains and grain boundaries can be calculated using the Arrhenius law[41]:

$$\sigma_{AC} = \sigma_o \exp(-E_a/k_B T) \quad (1)$$

where σ_{AC} is the AC conductivity, σ_o is the pre-exponential term, E_a is the activation energy, and κ_B (J/K) and T are the Boltzmann constant and absolute temperature (K), respectively. According to Eq. (1), the values of activation energies (E_g for grain, E_{gb} for grain boundary and E_s for surface) can be calculated by fitting the curves in Fig. 10. Both E_g and E_{gb} values of NECTO ceramics had different trends with the change of sintering temperature, as displayed in the Fig. 10a. The E_g of NECTO-950, NECTO-975 and NECTO-1000 ceramics were 0.110, 0.092 and 0.0868 eV, respectively. A slight decrease in E_g is consistent with the increase of grain conductivity shown in the Table 2. Meanwhile, with the increase of sintering temperature, the E_{gb} values of NECTO ceramics were 0.480, 0.747 and 0.739 eV, respectively. As shown in the Fig. 10b, the observed E_g values of NSCTO-900, NSCTO-975 and NSCTO-1000 ceramics were 0.0947, 0.0942 and 0.0837 eV, respectively, while the observed E_{gb} values were 0.502, 0.493 and 0.783 eV, respectively. The E_g values of NECTO and NSCTO ceramics were basically similar to the values of high-frequency relaxation activation energy obtained in Fig. 8, which further indicated that the dielectric response in the high frequency region was related to the grain. The changing trend

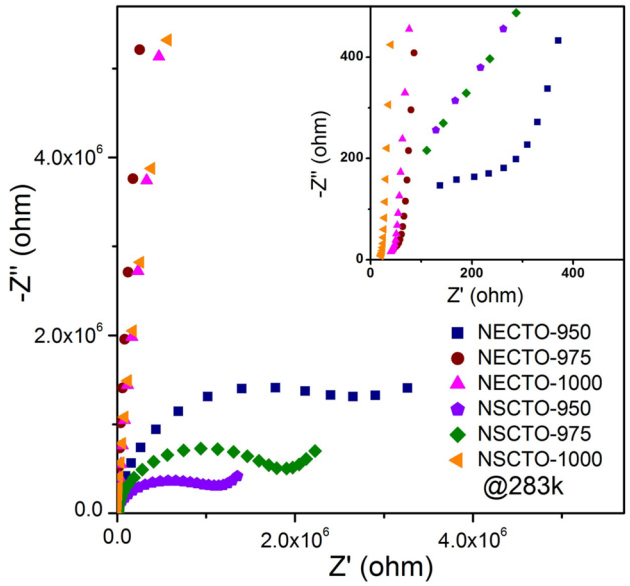

Figure 9. Impedance complex plane (Z*) plot at 283 K for $Na_{1/2}Eu_{1/2}Cu_3Ti_4O_{12}$ and $Na_{1/2}Sm_{1/2}Cu_3Ti_4O_{12}$ ceramics with different sintering temperature. Inset shows an expanded view of the Z* plot at 283 K in high frequency range.

Sample	Sintering temperature (°C)	R_g (Ω)	R_{gb} (Ω)	R_s (Ω)	E_g (eV)	E_{gb} (eV)	E_s (eV)
NECTO	950	338	3.11×10^6	2.76×10^6	0.110	0.480	0.454
	975	68.2	2.44×10^8	–	0.0920	0.747	–
	1000	48.2	2.34×10^8	–	0.0868	0.739	–
NSCTO	950	1091	8.12×10^5	7.9×10^5	0.0947	0.502	0.648
	975	961	1.79×10^6	1.39×10^6	0.0942	0.493	0.579
	1000	34.3	9.51×10^7	–	0.0837	0.783	–

Table 2. Grain resistance (R_g), grain boundary resistance (R_{gb}), surface resistance (R_s) and various activation energies (E_g for grain, E_{gb} for grain boundary and E_s for surface) data for $Na_{1/2}Eu_{1/2}Cu_3Ti_4O_{12}$ and $Na_{1/2}Sm_{1/2}Cu_3Ti_4O_{12}$ ceramics prepared at different temperature. The resistance data were obtained by fitting the impedance spectra in Fig. 9 using equivalent R(RQ) circuit.

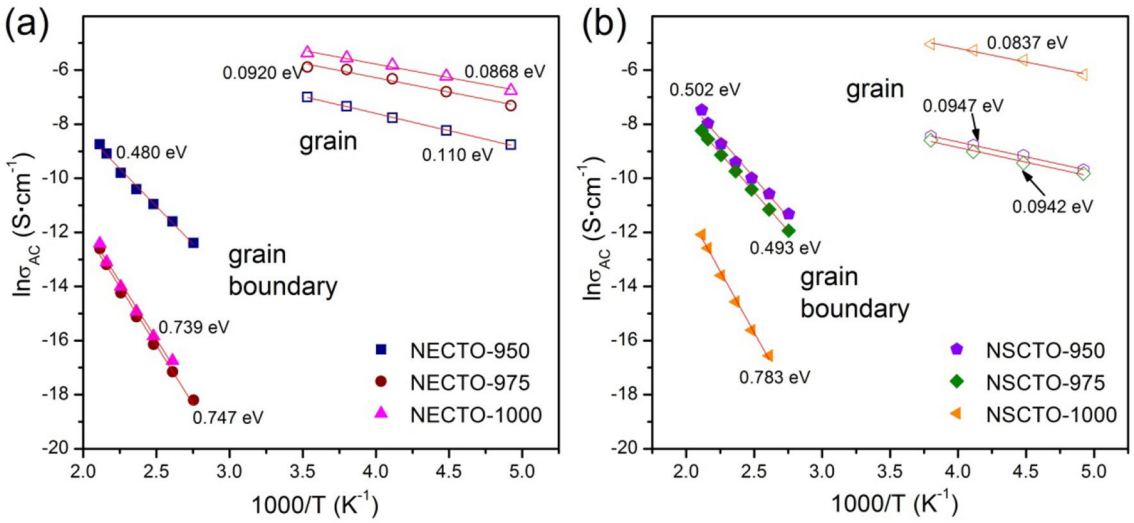

Figure 10. Arrhenius plots for the temperature dependence of σ_{AC} for (**a**) NECTO and (**b**) NSCTO samples. Red solid lines are the linear fitting curves.

of E_g and E_{gb} values of NSCTO samples with sintering temperature was very similar to that of NECTO samples. Compared with NECTO-950, NSCTO-950 and NSCTO-975 ceramics sintered at low temperature, E_{gb} and E_g values of the other ceramics prepared at high sintering temperature differed significantly, indicating that the IBLC polarization mechanism was formed, which will caused the giant dielectric response observed in NECTO-975, NECTO-1000 and NSCTO-1000 ceramics. The calculated E_{gb} and E_g values were nearly same as other reported in CCTO and TiO_2-related ceramics[29,49–51].

However, the abnormal high dielectric constant and dielectric loss observed in the low frequency for NECTO-950, NSCTO-950 and NSCTO-975 ceramics (shown in the Fig. 7) cannot be attributed to the IBLC effect. According to the analysis of Fig. 8, it could be governed by the polarization mechanism of SBLC. To confirm the possible source of the abnormal dielectric response in these ceramics, impedance complex spectrum of variable temperature (343–423 K) was displayed in the Fig. 11a–c, respectively. Because polycrystalline ceramic materials generally exhibit grain, grain boundary or surface impedances[23], they can be represented by the equivalent circuit shown in Fig. 11b. Meanwhile, the Arrhenius plots of ac conductivity (σ_{AC}) for these three samples displayed in the Fig. 11d. It was observed that a new diameter of the semicircle arcs of the NECTO-950, NSCTO-950 and NSCTO-975 samples in the low frequency decreased with increasing temperature, which was a thermal activation process. As displayed in the Fig. 11d and Table 2, the activation energy of $Na_{1/2}Eu_{1/2}Cu_3Ti_4O_{12}$ and $Na_{1/2}Sm_{1/2}Cu_3Ti_4O_{12}$ ceramics sintered at 950 or 975 °C were 0.454, 0.648 and 0.579 eV, respectively. Considering the activation energy obtained in Fig. 11d, this thermal excitation process at low frequency region did not represent the electrical response of the grain or grain boundary, but was caused by the surface effect[12,36,38]. It was indicated that abnormal dielectric response for NECTO-950, NSCTO-950 and NSCTO-975 ceramics could be attributed to interfacial polarization based on SBLC effect. This was also consistent with the result obtained in Fig. 8. Interestingly, the doping of (Na^+, Eu^{3+}) or (Na^+, Sm^{3+}) in CCTO lattice could induce the appearance of Cu^+ and Ti^{3+} in the grain during the sintering process. The low concentration of variable valence ions in the lattice could result in a small conductivity inside the grain at relatively low sintering temperature (950 °C). The abnormal permittivity and dielectric loss was contributed from the SBLC polarization mechanism for NECTO-950 and NSCTO-950 ceramics. NECTO and NSCTO ceramics prepared at high sintering temperature (1000 °C)

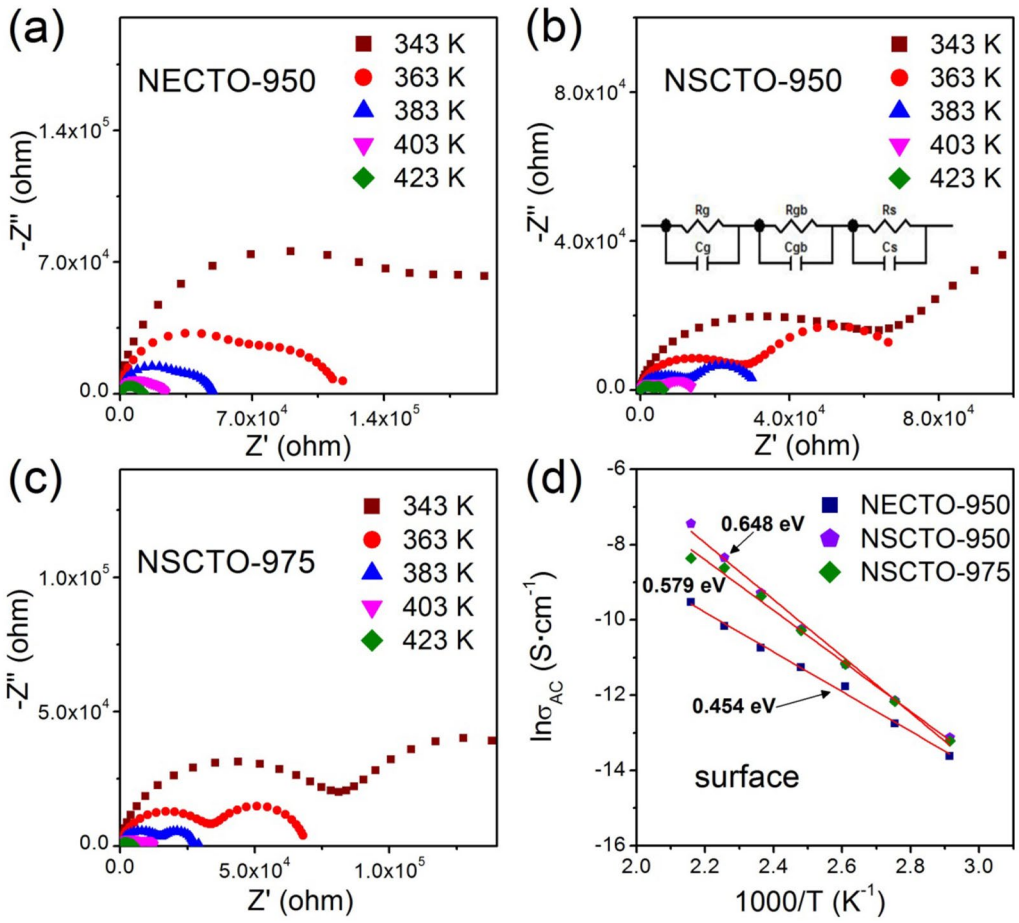

Figure 11. Impedance complex plane plots in the temperature range of 343–423 K for (**a**) NECTO-950, (**b**) NSCTO-950 and (**c**) NSCTO-975 ceramics; (**d**) Arrhenius plots of ac conductivity (σ_{AC}) for these three samples. Red solid lines are the linear fitting curves. Equivalent circuit indicated in frame (**b**) is used to represent the electrical properties of grain, grain boundary and surface effects.

would have more charge carriers with the increase of Cu^{+} and Ti^{4+} ions in ceramic structure, resulting in the formation of semiconductive region inside the grain. So, the giant dielectric constant and low dielectric loss for NECTO-1000 and NSCTO-1000 ceramics had been derived from an IBLC effect. According to the conclusion of XPS, the doping of (Na^{+}, Eu^{3+}) in CCTO-based ceramic was more likely to produce Cu^{+} ions than the doping of (Na^{+}, Sm^{3+}) in these ceramic. Therefore, the IBLC polarization mechanism appeared in the NECTO-975 ceramic containing high concentration of Cu^{+}, and the ceramic showed good dielectric stability. On the contrary, SBLC polarization mechanism appeared in NSCTO-975 with abnormal dielectric response, while Cu^{+} ion was relatively low in the ceramic. In summary, the number of charge carriers (vacancies or free electrons) in the ceramic lattice will impress the conductivity of the grains, resulting in a competitive coexistence between SBLC and IBLC effects, thereby affecting the dielectric properties of ceramic.

Conclusion

This work systematically dealt with the structural, ion valence and dielectric properties of $Na_{1/2}Eu_{1/2}Cu_3Ti_4O_{12}$ and $Na_{1/2}Sm_{1/2}Cu_3Ti_4O_{12}$ ceramics sintered at different temperature. According to the XRD and RS data, all ceramics showed a single phase of CCTO-related ceramics. The substitutions of (Na^{+}, Eu^{3+}) or (Na^{+}, Sm^{3+}) in the CCTO lattice could induce the appearance of Cu^{+} and Ti^{3+} in grain. The higher sintering temperature, the more content of Cu^{+} and Ti^{3+}, and the higher conductivity of grain in $Na_{1/2}Eu_{1/2}Cu_3Ti_4O_{12}$ and $Na_{1/2}Sm_{1/2}Cu_3Ti_4O_{12}$ ceramics, which also led to the gradual transformation of the polarization mechanism inside the ceramics from SBLC to IBLC. Therefore, $Na_{1/2}Eu_{1/2}Cu_3Ti_4O_{12}$ and $Na_{1/2}Sm_{1/2}Cu_3Ti_4O_{12}$ ceramics sintered at 1000 °C had giant dielectric permittivity of about 10^4, a low dielectric loss of about 10^{-2} and good frequency stability of about 10^2–10^6 Hz. At the same sintering temperature, the doping of Eu ions in the $Na_{1/2}Ln_{1/2}Cu_3Ti_4O_{12}$ system would induce from more Cu^{+} ions inside the ceramics than the doping of Sm ions during the process of preparation. This resulted in a more pronounced IBLC polarization mechanism in $Na_{1/2}Eu_{1/2}Cu_3Ti_4O_{12}$ ceramics than in $Na_{1/2}Sm_{1/2}Cu_3Ti_4O_{12}$ ceramics. Therefore, $Na_{1/2}Eu_{1/2}Cu_3Ti_4O_{12}$ ceramic prepared at 975 °C had better dielectric stability than $Na_{1/2}Sm_{1/2}Cu_3Ti_4O_{12}$ ceramic sintered at same temperature.

Data availability

All data generated or analysed during this study are included in this published article.

Received: 20 July 2023; Accepted: 12 September 2023
Published online: 15 September 2023

References

1. Wang, L. *et al.* Study on the preparation and mechanical properties of purple ceramics. *Sci. Rep.* **13**, 8755. https://doi.org/10.1038/s41598-023-35957-0 (2023).
2. Cao, Z., An, S. & Song, X. Effect of thermal treatment at high temperature on phase stability and transformation of Yb_2O_3 and Y_2O_3 co-doped ZrO_2 ceramics. *Sci. Rep.* **12**, 9955. https://doi.org/10.1038/s41598-022-13705-0 (2022).
3. Du, C. *et al.* Fabrication of high radiation efficiency dielectric resonator antenna array using temperature stable $0.8Zn_2SiO_4$–$0.2TiO_2$ microwave dielectric ceramic. *Adv. Mater. Technol.* **8**, 2201985. https://doi.org/10.1002/admt.202201985 (2023).
4. Chen, Z., Zheng, Y. & Li, B. A new microwave dielectric ceramic $TmVO_4$ with high-quality factor and the effect of TiO_2 on its microwave dielectric properties. *J. Mater. Sci. Mater. Electron.* **34**, 828. https://doi.org/10.1007/s10854-023-10254-8 (2023).
5. Boonlakhorn, J., Chanlek, N., Suksangrat, P., Thongbai, P. & Srepusharawoot, P. Colossal dielectric properties of $Na_{1/3}Ca_{1/3}Sm_{1/3}Cu_3Ti_4O_{12}$ ceramics: Computational and experimental investigations. *Ceram. Int.* **49**, 1690–1699. https://doi.org/10.1016/j.ceramint.2022.09.131 (2023).
6. Li, Z., Wu, J. & Wu, W. Composition dependence of colossal permittivity in $(Sm_{0.5}Ta_{0.5})xTi_{1-x}O_2$ ceramics. *J. Mater. Chem. C* **3**, 9206–9216. https://doi.org/10.1039/c5tc01659b (2015).
7. Tang, H., Zhou, Z. & Sodano, H. A. Relationship between $BaTiO_3$ nanowire aspect ratio and the dielectric permittivity of nanocomposites. *ACS Appl. Mater. Interfaces* **6**, 5450. https://doi.org/10.1021/am405038r (2014).
8. Saengvong, P. *et al.* Effects of sintering conditions on giant dielectric and nonlinear current–voltage properties of TiO_2-excessive $Na_{1/2}Y_{1/2}Cu_3Ti_{4.1}O_{12}$ ceramics. *Molecules* **27**, 5311. https://doi.org/10.3390/molecules27165311 (2022).
9. Xu, B., Zhang, J., Tian, Z. & Yuan, S. L. Synthesis, dielectric and nonlinear electrical properties of $Na_{1/2}Bi_{1/2}Cu_3Ti_4O_{12}$ ceramics by a sol–gel technique. *Mater. Lett.* **75**, 87–90. https://doi.org/10.1016/j.matlet.2012.01.025 (2012).
10. Schmidt, R. *et al.* Effects of sintering temperature on the internal barrier layer capacitor (IBLC) structure in $CaCu_3Ti_4O_{12}$ (CCTO) ceramics. *J. Eur. Ceram. Soc.* **32**, 3313–3323. https://doi.org/10.1016/j.jeurceramsoc.2012.03.040 (2012).
11. Subramanian, M. A., Li, D., Duan, N., Reisner, B. A. & Sleight, A. W. High dielectric constant in $ACu_3Ti_4O_{12}$ and $ACu_3Ti_3FeO_{12}$ phases. *J. Solid State Chem.* **151**, 323–325. https://doi.org/10.1006/jssc.2000.8703 (2000).
12. Variar, L., Muralidharan, M. N., Narayanankutty, S. K. & Ansari, S. High dielectric constant and low-loss, carbon black/$CaCu_3Ti_4O_{12}$/epoxy composites for embedded capacitor applications. *Mater. Res. Bull.* **152**, 111835. https://doi.org/10.1016/j.materresbull.2022.111835 (2022).
13. Li, J., Liang, P., Yi, J., Chao, X. & Yang, Z. Phase formation and enhanced dielectric response of $Y_{2/3}Cu_3Ti_4O_{12}$ ceramics derived from the Sol–Gel process. *J. Am. Ceram. Soc.* **98**, 795–803. https://doi.org/10.1111/jace.13355 (2015).
14. Kotb, H. M., Ahmad, M. M., Ansari, S. A., Kayed, T. S. & Alshoaibi, A. Dielectric properties of colossal-dielectric-constant $Na_{1/2}La_{1/2}Cu_3Ti_4O_{12}$ ceramics prepared by spark plasma sintering. *Molecules* **27**, 779. https://doi.org/10.3390/molecules27030779 (2022).
15. Gecil Evangeline, T. & Raja Annamalai, A. Dielectric properties of conventional and microwave sintered Lanthanum doped $CaCu_3Ti_4O_{12}$ ceramics for high-frequency applications. *Ceram. Int.* **48**, 25705–25713. https://doi.org/10.1016/j.ceramint.2022.05.179 (2022).
16. Liang, P., Yang, Z., Chao, X., Liu, Z. & Chen, X. M. Giant dielectric constant and good temperature stability in $Y_{2/3}Cu_3Ti_4O_{12}$ ceramics. *J. Am. Ceram. Soc.* **95**, 2218–2225. https://doi.org/10.1111/j.1551-2916.2012.05152.x (2012).
17. Boonlakhorn, J., Manyam, J., Krongsuk, S., Thongbai, P. & Srepusharawoot, P. Enhanced dielectric properties with a significantly reduced loss tangent in (Mg^{2+}, Al^{3+}) co-doped $CaCu_3Ti_4O_{12}$ ceramics: DFT and experimental investigations. *RSC Adv.* **11**, 25038–25046. https://doi.org/10.1039/d1ra02896k (2021).
18. Jumpatam, J. *et al.* Effects of Mg^{2+} doping ions on giant dielectric properties and electrical responses of $Na_{1/2}Y_{1/2}Cu_3Ti_4O_{12}$ ceramics. *Ceram. Int.* **42**, 16287–16295. https://doi.org/10.1016/j.ceramint.2016.07.167 (2016).

19. Mahfoz Kotb, H. & Ahmad, M. M. Electrical and dielectric properties of $Na_{1/2}La_{1/2}Cu_3Ti_4O_{12}$ ceramics prepared by high energy ball-milling and conventional sintering. *Chin. Phys. B* **25**, 128201. https://doi.org/10.1088/1674-1056/25/12/128201 (2016).
20. Jumpatam, J. *et al.* Significantly improving the giant dielectric properties of $CaCu_3Ti_4O_{12}$ ceramics by co-doping with Sr^{2+} and F^- ions. *Mater. Res. Bull.* **133**, 111043. https://doi.org/10.1016/j.materresbull.2020.111043 (2021).
21. Jumpatam, J., Boonlakhorn, J., Putasaeng, B., Chanlek, N. & Thongbai, P. Preparation, characterizations, dielectric properties and nonlinear behavior of $(Na^{+1/3}Ca^{2+1/3}Yb^{3+1/3})Cu_3Ti_4O_{12}$ ceramics. *Solid State Sci.* **132**, 106994. https://doi.org/10.1016/j.solidstatesciences.2022.106994 (2022).
22. Adams, T. B., Sinclair, D. C. & West, A. R. Giant barrier layer capacitance effects in $CaCu_3Ti_4O_{12}$ ceramics. *Adv. Mater.* **14**, 1321–1323 (2002).
23. Sinclair, D. C., Adams, T. B., Morrison, F. D. & West, A. R. $CaCu_3Ti_4O_{12}$: One-step internal barrier layer capacitor. *Appl. Phys. Lett.* **80**, 2153–2155. https://doi.org/10.1063/1.1463211 (2002).
24. Lindman, A., Helgee, E. E. & Wahnström, G. Comparison of space-charge formation at grain boundaries in proton-conducting $BaZrO_3$ and $BaCeO_3$. *Chem. Mater.* **29**, 7931–7941. https://doi.org/10.1021/acs.chemmater.7b02829 (2017).
25. Hu, W. *et al.* Electron-pinned defect-dipoles for high-performance colossal permittivity materials. *Nat. Mater.* **12**, 821. https://doi.org/10.1038/nmat3691 (2013).
26. Nachaithong, T., Thongbai, P. & Maensiri, S. Colossal permittivity in $(In_{1/2}Nb_{1/2})_xTi_{1-x}O_2$ ceramics prepared by a glycine nitrate process. *J. Eur. Ceram. Soc.* **37**, 655–660. https://doi.org/10.1016/j.jeurceramsoc.2016.09.006 (2017).
27. Kum-onsa, P., Thongbai, P., Putasaeng, B., Yamwong, T. & Maensiri, S. $Na_{1/3}Ca_{1/3}Bi_{1/3}Cu_3Ti_4O_{12}$: A new giant dielectric perovskite ceramic in $ACu_3Ti_4O_{12}$ compounds. *J. Eur. Ceram. Soc.* **35**, 1441–1447. https://doi.org/10.1016/j.jeurceramsoc.2014.11.028 (2015).
28. Jumpatam, J. *et al.* Non-ohmic properties and electrical responses of grains and grain boundaries of $Na_{1/2}Y_{1/2}Cu_3Ti_4O_{12}$ ceramics. *J. Am. Ceram. Soc.* **100**, 157–166. https://doi.org/10.1111/jace.14473 (2017).
29. Boonlakhorn, J., Kidkhunthod, P., Chanlek, N. & Thongbai, P. (Al^{3+}, Nb^{5+}) co–doped $CaCu_3Ti_4O_{12}$: An extended approach for acceptor–donor heteroatomic substitutions to achieve high–performance giant–dielectric permittivity. *J. Eur. Ceram. Soc.* **38**, 137–143. https://doi.org/10.1016/j.jeurceramsoc.2017.08.040 (2018).
30. Qiu, Y. *et al.* Grain size effect on the giant dielectric and nonlinear electrical behaviors of $Bi_{1/2}Na_{1/2}Cu_3Ti_4O_{12}$ ceramics. *Appl. Phys. A* **107**, 379–383. https://doi.org/10.1007/s00339-012-6806-9 (2012).
31. Boonlakhorn, J. *et al.* Dielectric properties with high dielectric permittivity and low loss tangent and nonlinear electrical response of sol-gel synthesized $Na_{1/2}Sm_{1/2}Cu_3Ti_4O_{12}$ perovskite ceramic. *J. Eur. Ceram. Soc.* **42**, 5659–5668. https://doi.org/10.1016/j.jeurceramsoc.2022.06.030 (2022).
32. Somphan, W., Thongbai, P., Yamwong, T. & Maensiri, S. High Schottky barrier at grain boundaries observed in $Na_{1/2}Sm_{1/2}Cu_3Ti_4O_{12}$ ceramics. *Mater. Res. Bull.* **48**, 4087–4092. https://doi.org/10.1016/j.materresbull.2013.06.028 (2013).
33. Thongbai, P., Yamwong, T. & Maensiri, S. Dielectric properties and electrical response of grain boundary of $Na_{1/2}La_{1/2}Cu_3Ti_4O_{12}$ ceramics. *Mater. Res. Bull.* **47**, 432–437. https://doi.org/10.1016/j.materresbull.2011.10.027 (2012).
34. Kolev, N. *et al.* Raman spectroscopy of $CaCu_3Ti_4O_{12}$. *Phys. Rev. B* **66**, 132102. https://doi.org/10.1103/PhysRevB.66.132102 (2002).
35. Capsoni, D. *et al.* Role of doping and CuO segregation in improving the giant permittivity of $CaCu_3Ti_4O_{12}$. *J. Solid State Chem.* **177**, 4494–4500. https://doi.org/10.1016/j.jssc.2004.09.009 (2004).
36. Lunkenheimer, P., Fichtl, R., Ebbinghaus, S. G. & Loidl, A. Nonintrinsic origin of the colossal dielectric constants in $CaCu_3Ti_4O_{12}$. *Phys. Rev. B* **70**, 172102. https://doi.org/10.1103/PhysRevB.70.172102 (2004).
37. De la Rubia, M. A. *et al.* Dielectric behaviour of Hf-doped $CaCu_3Ti_4O_{12}$ ceramics obtained by conventional synthesis and reactive sintering. *J. Eur. Ceram. Soc.* **32**, 1691–1699. https://doi.org/10.1016/j.jeurceramsoc.2012.01.024 (2012).
38. Hu, W. *et al.* Colossal dielectric permittivity in (Nb+Al) codoped rutile TiO_2 ceramics: Compositional gradient and local structure. *Chem. Mater.* **27**, 4934–4942. https://doi.org/10.1021/acs.chemmater.5b01351 (2015).
39. Biesinger, M. C., Lau, L. W. M., Gerson, A. R. & Smart, R. S. C. Resolving surface chemical states in XPS analysis of first row transition metals, oxides and hydroxides: Sc, Ti, V, Cu and Zn. *Appl. Surf. Sci.* **257**, 887–898. https://doi.org/10.1016/j.apsusc.2010.07.086 (2010).
40. Morita, Y. *et al.* Valence fluctuations and correlated metallic states in A-site ordered perovskite oxides $ACu_3V_4O_{12}$ (A=Na, Ca, and Y). *Phys. Rev. B* **81**, 165111. https://doi.org/10.1103/PhysRevB.81.165111 (2010).
41. Liu, Z., Chao, X., Liang, P., Yang, Z. & Zhi, L. Differentiated electric behaviors of $La_{2/3}Cu_3Ti_4O_{12}$ ceramics prepared by different methods. *J. Am. Ceram. Soc.* **97**, 2154–2163. https://doi.org/10.1111/jace.12940 (2014).
42. Li, M. *et al.* Origin(s) of the apparent high permittivity in $CaCu_3Ti_4O_{12}$ ceramics: clarification on the contributions from internal barrier layer capacitor and sample-electrode contact effects. *J. Appl. Phys.* **106**, 104106. https://doi.org/10.1063/1.3253743 (2009).
43. Thongbai, P., Jumpatam, J., Putasaeng, B., Yamwong, T. & Maensiri, S. The origin of giant dielectric relaxation and electrical responses of grains and grain boundaries of W-doped $CaCu_3Ti_4O_{12}$ ceramics. *J. Appl. Phys.* **112**, 114115. https://doi.org/10.1063/1.4768468 (2012).
44. Liu, J. *et al.* Large dielectric constant and Maxwell–Wagner relaxation in$Bi_{2/3}Cu_3Ti_4O_{12}$. *Phys. Rev. B* **70**, 144106. https://doi.org/10.1103/PhysRevB.70.144106 (2004).
45. Ni, L. & Chen, X. M. Enhancement of giant dielectric response in $CaCu_3Ti_4O_{12}$ ceramics by Zn substitution. *J. Am. Ceram. Soc.* **93**, 184–189. https://doi.org/10.1111/j.1551-2916.2009.03384.x (2010).
46. Somphan, W., Sangwong, N., Yamwong, T. & Thongbai, P. Giant dielectric and electrical properties of sodium yttrium copper titanate: $Na_{1/2}Y_{1/2}Cu_3Ti_4O_{12}$. *J. Mater. Sci. Mater. Electron.* **23**, 1229–1234. https://doi.org/10.1007/s10854-011-0578-4 (2011).
47. Thongbai, P., Jumpatam, J., Yamwong, T. & Maensiri, S. Effects of Ta^{5+} doping on microstructure evolution, dielectric properties and electrical response in $CaCu_3Ti_4O_{12}$ ceramics. *J. Eur. Ceram. Soc.* **32**, 2423–2430. https://doi.org/10.1016/j.jeurceramsoc.2012.02.048 (2012).
48. Yuan, L. *et al.* CdO–CuO–TiO_2 ternary dielectric systems: Subsolidus phase diagram and the effects of Cu segregation. *J. Eur. Ceram. Soc.* **38**, 4978–4985. https://doi.org/10.1016/j.jeurceramsoc.2018.07.038 (2018).
49. Zheng, P., Zhang, J. L., Shao, S. F., Tan, Y. Q. & Wang, C. L. Piezoelectric properties and stabilities of CuO-modified Ba(Ti, Zr)O_3 ceramics. *Appl. Phys. Lett.* **94**, 032902. https://doi.org/10.1063/1.3072347 (2009).
50. Bharti, B., Kumar, S., Lee, H.-N. & Kumar, R. Formation of oxygen vacancies and Ti^{3+} state in TiO_2 thin film and enhanced optical properties by air plasma treatment. *Sci. Rep.* **6**, 32355. https://doi.org/10.1038/srep32355 (2016).
51. Wang, C. *et al.* Relaxor-like behaviors in $Na_{1/2}Bi_{1/2}Cu_3Ti_4O_{12}$ ceramics. *J. Am. Ceram. Soc.* **100**, 2016–2023. https://doi.org/10.1111/jace.14720 (2017).

Acknowledgements

This work was financially supported in part by Youth Science Foundation of Guizhou Province Education Ministry (QJHKY[2020]098), Scientific Research Foundation of Guizhou Province (QKHPTRC[2018]5784-02) and Doctor Foundation of Zunyi Normal collage (ZSBS[2019]03).

Author contributions

L.-F.Y. and D.-D.H. did the material prepared/characterizations and electrical measurements of the samples. L.-F.Y. and T.Z. clarified the experimental data and came out with the manuscript. L.-F.Y. is the group leader and conducted the investigation of this work. All authors reviewed the manuscript.

Competing interests

The authors declare no competing interests.

Additional information

Correspondence and requests for materials should be addressed to L.-F.Y.

Reprints and permissions information is available at www.nature.com/reprints.

Publisher's note Springer Nature remains neutral with regard to jurisdictional claims in published maps and institutional affiliations.